Journal Name

ARTICLE TYPE

Cite this: DOI: 00.0000/xxxxxxxxxx

Biexcitons in CdSe Nanoplatelets: Geometry, Binding Energy and Radiative Rate†

David F. Macias-Pinilla,[a,b] Josep Planelles,[b] and Juan I. Climente *[b]

Received Date
Accepted Date

DOI: 00.0000/xxxxxxxxxx

Biexciton properties in semiconductor nanostructures are highly sensitive to quantum confinement, relative electron-hole masses, dielectric environment and Coulomb correlations. Here we present a variational Quantum Monte Carlo model which, coupled to effective mass Hamiltonians, takes into account all of the above effects. The model is used to provide theoretical assessment on the biexciton ground state properties in colloidal CdSe nanoplatelets. A number of characteristic features is observed: (i) the finite thickness of these systems makes the biexciton geometry depart from the planar square expected in the two-dimensional (2D) limit, and form a distorted tetrahedron instead; (ii) the strong dielectric confinement enhances not only Coulomb attractions but also repulsions, which lowers the ratio of biexciton-to-exciton binding energy down to $E_b^{XX}/E_b^X = 0.07$. (iii) E_b^{XX} is less sensitive than E_b^X to lateral confinement, and yet it can reach values above 30 meV, thus granting room temperature stability; (iv) the ratio of biexciton-to-exciton radiative rates, k_{XX}^{rad}/k_X^{rad}, decreases from 3.5 to ∼1 as the platelet area increases. These results pave the way for rational design of biexciton properties in metal chalcogenide nanoplatelets.

1 Introduction

The control achieved in the last years concerning composition, size and shape over colloidal semiconductor nanocrystals offers a wide range of possibilities to tune and improve their optoelectronic properties.[1] In particular, the development of quasi-2D nanoplatelets (NPLs) has gathered much interest because of their outstanding photophysical properties, which make them promising building blocks for optical applications.[2–5] Among other aspects, intensive research is currently focused on the nature of biexciton (XX) states in NPLs. The weak lateral confinement in these structures make Auger processes slower than in quantum dots,[6–9] while the strong confinement in the out-of-plane direction provides strong excitonic binding energies.[10–13] Altogether, this is expected to lead to room temperature stable, highly emissive XX states,[14,15] which are of interest for low threshold and continuous wave lasing[10,16] energy harvesting[13,17] and source of entangled photon pairs.[18]

Understanding the electronic structure of XX in NPLs is of clear interest for further progress. Several theoretical studies have dealt with XX in semiconductors in the past. Because the properties of single excitons (X) are better understood, the ratio E_b^{XX}/E_b^X –with E_b^X the single exciton binding energy– is often taken as a referent value to visualize how different the XX behavior is. Obviously, because X-X (electron-hole) interactions are of dipole-dipole (monopole-monopole) kind, $E_b^{XX}/E_b^X < 1$. Also, in general, variational models show that E_b^{XX}/E_b^X is dependent on the fraction between electron and hole masses, $\sigma = m_e/m_h$. In bulk, E_b^{XX}/E_b^X was estimated to be 0.3 when one carrier is much heavier than the other ($\sigma = 0$, hydrogen molecule limit) and decrease to 0.03 when both carriers have the same mass ($\sigma = 1$, positronium molecule limit).[19,20] The same trend was observed later on in calculations for 2D systems, except that here quantum confinement boosted XX binding energy, such that E_b^{XX}/E_b^X ranged from 0.56 to 0.14.[21]

Systematic experiments in epitaxial GaAs quantum wells with varying thickness reported a roughly constant value $E_b^{XX}/E_b^X \approx 0.2$.[22] This was about twice the value in bulk (the so-called Haynes rule in 3D[23]), thus confirming the enhancement of E_b^{XX} in quasi-2D systems. A simple and elegant rationalization of this result was given by Singh and co-workers.[24] They considered a biexciton geometry in which electrons and holes form a perfect square, with carriers of the same sign in opposite corners. Using effective mass Hamiltonians, they showed in a strictly 2D system, this geometry leads to $E_b^{XX}/E_b^X = 0.23$, regardless of the masses. This ratio has been sometimes taken as a rule in studies of XX in colloidal NPLs.[10,12] However, NPLs present some distinct features which demand revisiting this assumption. First, NPLs have a finite thickness (few atomic layers), hence departing from the strict 2D limit. Singh and co-workers recognized a few years later this could compromise the ideal square geometry.[25] Second, NPLs have finite lateral confinement. In epitaxial[26] and colloidal[27]

[a] Institute of Advanced Materials (INAM), Universitat Jaume I, Av. Sos Baynat, s/n, 12071 Castelló, Spain.
[b] Departament de Química Física i Analítica, Universitat Jaume I, Av. Sos Baynat, s/n, 12071 Castelló, Spain. E-mail:climente@uji.es

quantum dots, this has been shown to affect X and XX differently. Third, NPLs experience a strong dielectric mismatch, which was absent in epitaxial quantum wells. This may also affect X and XX differently, as noted in transition metal dichalcogenides.[28,29]

In this work we aim at describing XX states in colloidal NPLs and study the role of the aforementioned effects. We focus on CdSe NPLs, where highly emissive XX states have been reported.[10,13,14,30] An accurate description of XX states is challenging because it depends on the fine balance between attractions and repulsions, which is only achieved when Coulomb correlations are well captured.[31] Because NPLs are in an intermediate confinement regime, with strong Coulomb correlations,[32,33] the configuration interaction methods often used for quantum dots may fall short to this end. As an alternative, in the last years the authors have developed variational Quantum Monte Carlo (VQMC) methods, coupled to effective mass Hamiltonians, which have successfully described the ground state of single excitons[34] and trions in CdSe NPLs.[35] Here, we extend such models to the case of biexcitons, since the use of VQMC methods has proved useful in the study of XX in low-dimensional structures in the past.[36] We find that finite thickness, dielectric mismatch and lateral confinement are all relevant factors in determining the optoelectronical properties of XX, including its binding energy and radiative rate.

2 Theoretical Framework

We calculate the XX ground state energies and wave functions by extending the method proposed for excitons and trions in Refs. 34,35. Thus, a $k\cdot p$ Hamiltonian for two uncoupled (conduction and valence) bands is used:

$$H_{XX} = \sum_{i=e_1,e_2,h_a,h_b} \left(\frac{\hat{\mathbf{p}}_\perp^2}{2m_{\perp,i}} + \frac{\hat{p}_z^2}{2m_{z,i}} + V_i \right) + V_c(\mathbf{r}_{e_1},\mathbf{r}_{e_2}) + V_c(\mathbf{r}_{h_a},\mathbf{r}_{h_b}) + \sum_{i=e_1,e_2}\sum_{j=h_a,h_b} V_c(\mathbf{r}_i,\mathbf{r}_j) + 2E_{gap}, \quad (1)$$

where $m_\perp$ and $\hat{\mathbf{p}}_\perp$ are the in-plane effective mass and momentum operator, while m_z and $\hat{p}_z$ are the corresponding out-of-plane counterparts. The single particle potential is $V_i = V_i^{conf} + V_i^{self}$. Here, V_i^{conf} is the confining potential, which is zero inside the cuboidal NPL with dimensions $L_x \times L_y \times L_z$ (see Fig. 1a), and infinite outside. This (hard wall) confinement description is technically convenient and provides a reasonable approximation to the problem. The actual band-offset between the NPL and its surroundings is of few eV.[37] The resulting wave function penetration outside the NPL is then small, and its influence on the binding energies we study is scarce, since these are mostly in-plane Coulomb interactions. V_i^{self} is the self-energy potential that results from the interaction of the carriers with their image charges because of the dielectric mismatch between the NPL and the surrounding environment (commonly organic ligands).[38] $V_c(\mathbf{r}_i,\mathbf{r}_j)$ terms represent the Coulomb interaction between carriers. These take into account the polarization coming from the dielectric mismatch, again through the image charge method.[38] E_{gap} is the bulk band gap of CdSe.

Hamiltonian (1) is solved with a four-parameter variational wave function for the biexciton ground state:

$$\Psi_{XX}(\mathbf{r}_{e_1},\mathbf{r}_{e_2},\mathbf{r}_{h_a},\mathbf{r}_{h_b}) = N_{XX}\,\Phi_e(\mathbf{r}_{e_1})\Phi_e(\mathbf{r}_{e_2})\Phi_h(\mathbf{r}_{h_a})\Phi_h(\mathbf{r}_{h_b}) \times F(r_{1a},r_{1b},r_{2a},r_{2b},r_{12},r_{ab}), \quad (2)$$

where spin degrees of freedom are omitted. Here, N_{XX} is the normalization factor, Φ_e and Φ_h are the non-interacting electron and hole envelope functions, $\Phi_i = \prod_{\alpha=x,y,z}\cos(\pi\alpha/L_\alpha)$. F is the correlation factor, described by:

$$F(r_{1a},r_{1b},r_{2a},r_{2b},r_{12},r_{ab}) = e^{-Z\frac{(s_1+s_2)}{2}}\cosh\left(ZQ\frac{t_1-t_2}{2}\right) \times e^{Z\frac{\beta r_{12}}{1+Z\alpha r_{12}}}e^{Z\frac{\beta r_{ab}}{1+Z\alpha r_{ab}}}, \quad (3)$$

where $r_{12}, r_{ab}, r_{1a}, r_{1b}, r_{2a}, r_{2b}$ are *in-plane* interparticle distances, $s_1 = r_{1a}+r_{1b}$, $s_2 = r_{2a}+r_{2b}$, $t_1 = r_{1a}-r_{1b}$ and $t_2 = r_{2a}-r_{2b}$. The variational parameters to optimize are Z, Q, β and α.

One can note Ψ_{XX} is reminiscent of the trial wave function used by Kleinman for quantum wells.[21] Thus, the first term in Eq. (3) describes Slater correlation factors, analogous to those used to account for carrier attraction of individual excitons.[32] Z can be seen as a scaling factor reflecting the strength of electron-hole attraction (its inverse can be related to an effective XX Bohr radius). In the second term, Q allows for a non-symmetric interaction in the biexciton, which makes the wave function flexible enough as to describe the limits of biexciton and of two weakly interacting excitons. The last two exponentials in Eq. (3), involving α and β parameters, are missing in Kleinman's wave function. They are Padé-Jastrow factors representing the carrier repulsion correlation. While they generally involve minor energetic corrections, they allow us to compare on equal footing with the variational function we have developed to study trions.[34,35]

For the sake of comparison, we also calculate the single X ground state. The Hamiltonian reads:

$$H_X = \sum_{i=e,h}\left(\frac{\hat{\mathbf{p}}_\perp^2}{2m_{\perp,i}} + \frac{\hat{p}_z^2}{2m_{z,i}} + V_i\right) + V_c(\mathbf{r}_e,\mathbf{r}_h) + E_{gap}, \quad (4)$$

and the excitonic wave function we use is:

$$\Psi_X(\mathbf{r_e},\mathbf{r}_h) = N_X\,\Phi_e(\mathbf{r}_e)\Phi_h(\mathbf{r}_h)e^{-Z_x r_{eh}}, \quad (5)$$

with r_{eh} being the electron-hole in-plane separation and Z_x (the inverse of the exciton Bohr radius) the only variational parameter.

A straight variational solution of Ψ_{XX} and Ψ_X is not viable because of the large number of dimensions and parameters, particularly in the XX case. We then resort to VQMC methods, as described in Ref. 34. A few considerations are worth for the XX case. In order to obtain a satisfactory importance sampling, it is convenient to initialize random walks by distributing the carriers in a square geometry in the center of the NPL –as assumed by Singh and co-workers[24]– with the square sides being close to the effective Bohr radius in 2D (see sketch in Fig. 1a). It is reasonable from an electrostatic point of view for this to be close to the optimal biexciton geometry. The Metropolis algorithm will then

determine any possible deviation from this initial guess. Random walks are taken in the space $(\mathbf{r}_{e_1}, \mathbf{r}_{e_2}, \mathbf{r}_{h_a}, \mathbf{r}_{h_b})$. The step length in the walk should be such as to provide 50% of accepted points. For this to happen, a few recursive thermalizations must be carried out before starting the sampling. Also, the use of Newton-Raphson methods for a rapid determination of the optimal variational parameters, which we have used for excitons and trions,[34] is found to be inefficient for XX. We suspect this is connected to the different sensitivity of the wavefunction to the four variational parameters, (Z, Q, α, β). In particular, the sensitivity to α and β is much smaller than that to Z. The small gradients in these directions likely lead to unreliable estimates of the steps needed for the optimization. As an alternative, a sequential optimization can be employed. First, we scan Z (the most influential parameter) for fixed, arbitrary values of Q, β and α. Next, we set Z to the value providing the lowest energy and scan over Q, β and α successively. This procedure is repeated with ever finer scan meshes, until sub-meV convergence of the ground state energy is achieved.

Once Ψ_{XX} and Ψ_X are optimized, the corresponding radiative recombination rates can be calculated within the dipole approximation.[39] The X rate is then given by:[32]

$$k_X^{rad} = \theta \frac{1}{2} |\langle 0|\delta_{\mathbf{r}_e,\mathbf{r}_h}|X\rangle|^2 = \theta \frac{1}{2} N_X^2 \prod_{\alpha=x,y,z} \left(\frac{L_\alpha}{2}\right)^2. \quad (6)$$

where θ is a constant of proportionality and the $1/2$ factor accounts for the spin selection rule (only half of the four-fold degenerate levels forming the exciton ground state are bright). In turn, the XX rate is given by:

$$k_{XX}^{rad} = \theta\, 2 \left|\langle \Psi_X |\delta_{\mathbf{r}_{e_2},\mathbf{r}_{h_b}}|\Psi_{XX}\rangle\right|^2 = \theta\, 2\, (N_X N_{XX} \mathscr{I})^2, \quad (7)$$

where the 2 factor accounts for the number of spin-allowed transitions (two for the singlet ground state), and:

$$\mathscr{I} = \int \Phi_e(\mathbf{r}_{e_1})^2 \Phi_e(\mathbf{r}_{e_2})^2 \Phi_h(\mathbf{r}_{h_a})^2 e^{-(\frac{Z}{2}+Z_x)r_{1a}} e^{-\frac{Z}{2}r_{12}} e^{-\frac{Z}{2}r_{2a}}$$

$$\times \cosh\Big(\frac{ZQ}{2}(r_{1a} - r_{12} - r_{2a})\Big) e^{Z\frac{\beta r_{12}}{1+Z\alpha r_{12}}} e^{Z\frac{\beta r_{2a}}{1+Z\alpha r_{2a}}} d\mathbf{r}_{e_1} d\mathbf{r}_{e_2} d\mathbf{r}_{h_a}, \quad (8)$$

is an integral that we calculate numerically using Monte Carlo routines.

A suite of Fortran codes implementing the methods described in this section and used for the calculations XX states in this work are provided in the Supplementary Information for free use. Those used to compute X and X^- (trion) states can be found in Ref. 34.

3 Results and Discussion

The target of our study is to describe the biexciton ground state in CdSe NPLs. We use the same material parameters as in earlier works dealing with excitons and trions, which provided reasonable agreement with experiments,[32,35,40] see Table 1. Because electron-hole correlations take place in the NPL plane, the relevant mass ratio is $\sigma = m_{\perp,e}/m_{\perp,h} = 0.54$, such that excitonic interactions are half way between hydrogen and positronium molecules.

Table 1 Parameters used in the calculations. Here, a_0 represents the lattice constant, ε_0 is the vacuum permittivity and m_0 is the free electron mass.

Parameter	CdSe	Units
ε_{NPL}	10[41]	ε_0
$m_{\perp,e}$	0.22[42]	m_0
$m_{\perp,h}$	0.41[42]	m_0
$m_{z,e}$	0.4[32]	m_0
$m_{z,h}$	0.9[32]	m_0
E_{gap}	1.67[41]	eV
a_0	6.08[41]	Å

3.1 Effect of dielectric confinement

The weak dielectric screening set by the ligands around the NPL results is an increase of the strength of Coulomb interactions within the NPLs, and therefore of the binding energies as compared to all-solid systems.[28,29,32,42,43] To our knowledge, there are no previous studies on how this affects XX in colloidal NPLs. To shed light on this point, we consider a prototypical CdSe NPL, with 4.5 monolayers (ML) thickness ($L_z = 1.37$ nm) and weak lateral confinement (L_x= 20 nm and $L_y = 2L_x$, see Fig.1a), and vary the dielectric constant of the outer medium, ε_{out}.

Figures 1(b) and (c) show the dependence of the binding energies of X and XX on ε_{out}. For X, the binding energy is defined as $E_b^X = E_e + E_h - E^X$, where $E_{e/h}$ is the energy of independent electron/hole and E^X the total exciton energy. For XX, the binding energy is $E_b^{XX} = 2E^X - E^{XX}$, with E^{XX} the total biexciton energy. In the absence of dielectric mismatch ($\varepsilon_{out} = \varepsilon_{NPL} = 10$), we obtain $E_b^{XX} = 8.8$ meV. This energy is greater than that in usual epitaxial quantum wells ($E_b^{XX} \approx 1$ meV)[22], which is consistent with the fact that quantum confinement is stronger in NPLs ($L_z = 1.37$ nm vs. $L_z = 8-16$ nm in the wells). The value is however smaller than those measured for actual (dielectrically mismatched) CdSe-based NPLs: $E_b^{XX} = 10-28$ meV in CdSe/CdS NPLs (mean value 16.5 meV)[13] or $E_b^{XX} = 30 \pm 5$ meV in core-only NPLs.[10] This discrepancy narrows down once dielectric confinement is taken into account. Fig. 1(c) shows that E_b^{XX} increases as ε_{out} is reduced. For typical organic ligands used in NPLs, $\varepsilon_{out} \approx 2$.[44–46] The calculated value of E_b^{XX} is then doubled, reaching $E_b^{XX} = 18-21$ meV. This energy is in closer agreement with the experiments, although the exact value may be underestimated in our simulations because the precise value of ε_{NPL} to be used in CdSe NPLs is uncertain. We use $\varepsilon_{NPL} = 10$, close to the static dielectric constant of bulk CdSe, but other works find good fits to experimental exciton and trion binding energies using the high frequency constant instead ($\varepsilon_{NPL} = 7.9$)[46] and even lower values, $\varepsilon_{NPL} = 6$ in Ref. 47. Regardless of the exact numbers, it is concluded from Fig. 1(b), (c) that dielectric confinement enhances not only E_b^X but also E_b^{XX}, leading to values comparable to experimental measurements.

Fig. 1(d) compares the emission energy of X, X^- and XX as a function of ε_{out}. It follows from the figure that the emission energy increases as ε_{out} departs from ε_{NPL}. This is in spite of E_b^X and E_b^{XX} becoming larger. The reason is that the (repulsive)

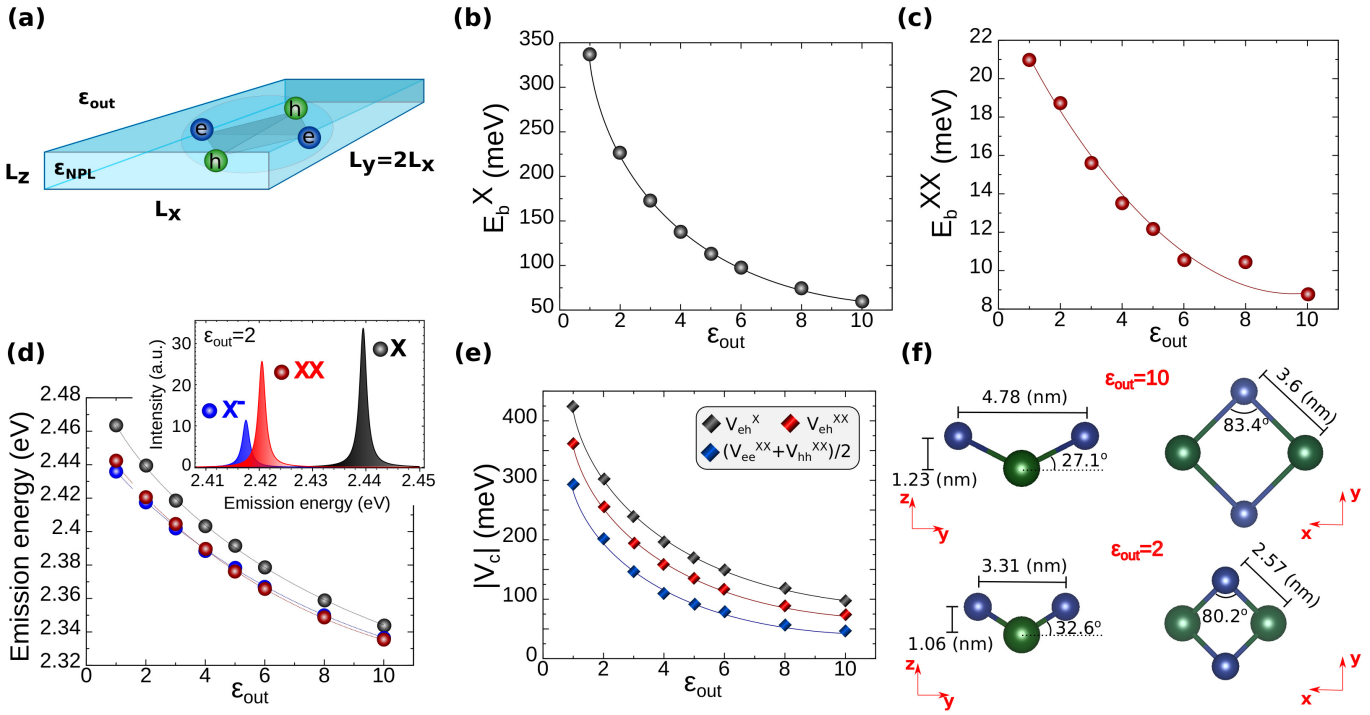

Fig. 1 (a) Sketch of the NPL under study. (b-e): effect of the dielectric mismatch on the energies of X and XX. (b) X binding energy. (c) XX binding energy. (d) X, X^- and XX emission energy, insets represent the transition probability with $\varepsilon_{out} = 2$. (e) Expectation values of Coulomb interactions in X and XX. (f) Schematic of the most likely XX geometry for $\varepsilon_{out} = 10$ and $\varepsilon_{out} = 2$. In (b,c,d and e), symbols are calculated values and lines are fits used to remove the scattering of the statistical estimates.

self-energy interaction, V_i^{self} in Eq. (1), is also stimulated by the dielectric confinement, and in practice it overcomes the enhancement of the (attractive) Coulomb interactions. The same behavior has been reported before in trions[35] and neutral excitons.[32,42] The figure also reveals that the XX binding energy is comparable to that of the trion, but it becomes slightly lower for small ε_{out} values. As a consequence, the calculated emission spectrum for $\varepsilon_{out} = 2$, plotted in the inset of Fig. 1(d), shows the XX peak in between those of X and X^-.

We have shown in Fig. 1(b), (c) that the dielectric confinement enhances the binding energies of both X and XX. It is worth noting, however, that the relative effect is smaller for XX. When $\varepsilon_{out} = 10$, the ratio of binding energies is $E_b^{XX}/E_b^X = 0.13$, and it decreases down to $E_b^{XX}/E_b^X = 0.07$ when $\varepsilon_{out} = 2$. These values are well below the $E_b^{XX}/E_b^X = 0.23$ ratio expected for a planar square in a 2D, dielectrically homogeneous system.[24] To explain this observation, we set the optimized variational parameters $(Z, Q, \alpha, \beta)_{opt}$ in Ψ_{XX} and carry out random walks with our VQMC codes. For each step in the walk, the values of $(\mathbf{r}_{e_1}, \mathbf{r}_{e_2}, \mathbf{r}_{h_a}, \mathbf{r}_{h_b})$ are stored. Because the Metropolis algorithm favors exploring the regions where the density probability is highest, the mean value of such coordinates is a direct probe of the equilibrium position for the XX particles. Figure 1(f) illustrates the resulting geometry calculated for two ε_{out} values. One can see that electrons and holes in XX form a nearly flat distorted tetrahedron, which is in between the expected distribution for a strict 2D system (planar square or tetragon)[24,25] and a fully 3D one (regular tetrahedron).[48] This is a consequence of the finite but small thickness of colloidal NPLs.

It is worth noting that the strong Coulomb interactions lift the xy-plane symmetry of the NPL potential. Permutation symmetries, $e_1 \leftrightarrow e_2$, $h_a \leftrightarrow h_b$, $(e_1, e_2) \leftrightarrow (h_a, h_b)$ are however preserved. It should be also noted that the precise geometry is dependent on the strength of dielectric confinement. As compared to the case without dielectric mismatch, $\varepsilon_{out} = 10$, the $\varepsilon_{out} = 2$ case implies not only shorter bond lengths, but also a greater departure from the planar square geometry (see angles in Fig. 1(f)).

Further insight into the small E_b^{XX}/E_b^X ratio is obtained by analyzing the Coulomb interaction energies for X and XX. The variational energy of X can be decomposed as:

$$E^X = \langle E_e^X \rangle + \langle E_h^X \rangle + \langle V_{eh}^X \rangle + E_{gap}. \quad (9)$$

Here $\langle E_j^X \rangle$, with $j = e, h$, is the expectation value of the electron/hole single-particle terms in Hamiltonian (4), and $\langle V_{eh}^X \rangle$ that of the Coulomb attraction term. In turn, the variational energy of XX is:

$$E^{XX} = 2\langle E_e^{XX} \rangle + 2\langle E_h^{XX} \rangle + 4\langle V_{eh}^{XX} \rangle + \langle V_{ee}^{XX} \rangle + \langle V_{hh}^{XX} \rangle + 2E_{gap}, \quad (10)$$

where the expectation values are now taken from Hamiltonian (1). We may approximate $\langle E_j^X \rangle \approx \langle E_j^{XX} \rangle \approx \langle E_j \rangle$, where E_j is the single-particle energy of carrier j in the absence of any Coulomb potentials. Then, from Eqs. (9) and (10), the binding energies can be expressed as:

$$E_b^X = -\langle V_{eh}^X \rangle, \quad (11)$$

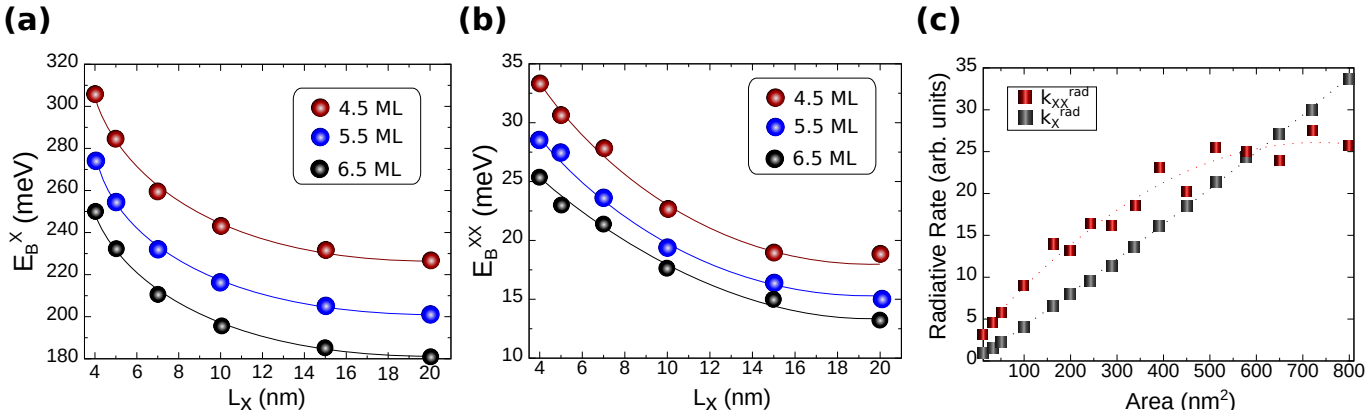

Fig. 2 Effect of the spatial confinement on the energies and recombination rates of X and XX. (a) Binding energy of X, for different thicknesses and lateral dimensions. (b) Same but for XX. (c) Radiative rates for a 4.5 ML NPL, as a function of the NPL area. Symbols are calculated values and lines are fits used to remove the scattering of the statistical estimates.

and

$$E_b^{XX} = 2\left[\langle V_{eh}^X\rangle - \left(2\langle V_{eh}^{XX}\rangle + \frac{\langle V_{ee}^{XX}\rangle + \langle V_{hh}^{XX}\rangle}{2}\right)\right]. \qquad (12)$$

These expressions evidence that E_b^X depends solely on the electron-hole attraction within X, while E_b^{XX} depends on the balance between attractions and repulsions. As observed in early studies of spherical QDs,[49] the self-energy terms (also called dielectric solvation energy) have no first order effect on E_b^{XX}.

Figure 1(e) shows the effect of the dielectric confinement on the absolute values of Coulomb expectation values. For X, reducing ε_{out} enhances $|\langle V_{eh}^X\rangle|$, which provides a large increase of E_b^X. For XX, however, reducing ε_{out} enhances not only the attraction terms, $|\langle V_{eh}^{XX}\rangle|$, but also the repulsion ones, $|\langle V_{ee}^{XX} + V_{hh}^{XX}\rangle|/2$. The compensation between attractions and repulsions in Eq. (12) implies that the increase of E_b^{XX} is only moderate.

3.2 Effect of thickness and lateral confinement

Current synthetic procedures for Cd chalcogenide NPLs enable controlling the thickness, usually from 3.5 to 8.5 atomic ML,[37,50,51] as well as the lateral dimensions, from tens to few nm.[51–53] Such changes in the strength of the confinement have been noted to be important in determining the binding energy[32,42,47,54] and radiative lifetimes of X.[50,53,55,56] Here we study how they affect XX.

Figs. 2(a) and (b) show the calculated values of E_b^X and E_b^{XX} in NPLs with different thicknesses and varying lateral confinement, L_x. As in the previous section, we consider that lateral confinement is anisotropic –which is often the case in experiments[52]– and fix $L_y = 2L_x$. Dielectric confinement is considered by setting $\varepsilon_{out} = 2$. The figures reveal that the binding energies of both X and XX increase with the confinement strength. By going from $L_x = 20$ nm (weakly confined NPL) to $L_x = 4$ nm (wire-like geometry), E_b^{XX} is almost doubled (from $E_b^{XX} = 18$ meV to $E_b^{XX} = 33.5$ meV, in the 4.5 ML NPL). This result indicates that lateral confinement provides a robust means of stabilizing XX, since it ensures that binding energies exceed thermal energy at room temperature.

All in all, the absolute change of E_b^{XX} with lateral confinement is smaller than that of E_b^X. This should translate into lesser sensivity in the emission spectrum energy. However, and contrary to the case of dielectric confinement (Fig. 1b), the relative increase of E_b^{XX} is greater than that of E_b^X. For example, in the case of 4.5 ML, a weakly confined NPLs ($L_x = 20$ nm) has a ratio $E_b^{XX}/E_b^X = 0.07$, but it increases up to 0.10 when a wire-like NPL is used instead ($L_x = 4$ nm). That is, in the same way that E_b^{XX}/E_b^X increases when moving from 3D to 2D,[21] it also increases when moving from 2D to quasi-1D. The influence of the thickness on E_b^{XX}/E_b^X, within the range under study (4.5-6.5 ML), is however minor. For weakly confined NPLs ($L_x = 20$ nm), we obtain $E_b^{XX}/E_b^X \approx 0.075$. For narrow ones ($L_x = 4$ nm), we obtain $E_b^{XX}/E_b^X \approx 0.10$. The scarce dependence on the thickness is reminiscent of observations in epitaxial quantum wells.[22]

It has been argued that lateral confinement in colloidal NPLs can have a great impact on the X oscillator strength through the so-called giant oscillator strength effect (GOST),[50,53,55,56] which was originally proposed for epitaxial quantum wells.[57] According to this effect, the oscillator strength (and hence the radiative rate) of X scales linearly with the NPL area. Robust experimental verification seems however lacking to date. It has been recently suggested that accidental localization of the X in CdSe NPLs prevents more clear manifestations.[58] At any rate, investigating how GOST affects the radiative rate of XX in ideal NPLs is of interest to guide eventual experimental developments in this line.

In Fig. 2c, we compare the radiative rates of X and XX, calculated in arbitrary units using Eqs. (6) and (7). A nearly linear increase with the NPL area, $A = L_x \times L_y = 2L_x^2$, is observed for k_X^{rad}, consistent with GOST. An increase can be also observed for k_{XX}^{rad}, but it appears to saturate as the area gets larger. For the smallest NPLs, Fig. 2c provides a ratio $k_{XX}^{rad}/k_X^{rad} = 3.5$. This is consistent with the expected behavior of strongly confined structures, where biexcitons have four as many spin-allowed recombinations channels than excitons. For the large NPLs, however, the ratio is reduced, reaching $k_{XX}^{rad}/k_X^{rad} < 1$ after 600 nm^2. These values are well below the factor of two expected in bimolecular descriptions of XX, sometimes assumed in studies of NPLs.[9] The quenching of the k_{XX}^{rad}/k_X^{rad} ratio is reminiscent of the trion behavior,[35,46] and is

related to the X-X correlations.

It can be concluded from Fig. 2c that radiative lifetimes of XX in CdSe NPLs should not be very different from those of X. Because the latter are usually in the few ns regime,[3,9] a similar figure should be expected for XX. This is consistent with the fact that XX decay in NPLs is found to be dominated by (non-radiative) Auger processes, which are often in the regime of hundred picoseconds.[8]

4 Conclusions

We have presented a VQMC-effective mass model which calculates the XX ground state in colloidal NPLs, including the effects of lateral and vertical quantum confinement, dielectric confinement, and Coulomb correlations. These are all necessary ingredients for a reliable description of the fine balance between attractions and repulsions in such systems.

We have used the model to investigate XX in CdSe NPLs. The XX geometry has been found to deviate from the planar square expected for strictly 2D systems, mainly because of the finite thickness and inhomogeneous dielectric environment. This invalidates the rule that $E_b^{XX}/E_b^X = 0.23$, which was proposed for 2D quantum wells[24] and has been occasionally accepted for NPLs.[10,12] The ratio E_b^{XX}/E_b^X is still roughly constant with the NPL thickness between 4.5 and 6.5 ML, but it increases with the lateral confinement and decreases with the dielectric confinement, with values $E_b^{XX}/E_b^X = 0.05 - 0.10$. For typical CdSe NPLs surrounded by organic ligands, E_b^{XX} is in the range of few tens of meV, and thus susceptible of being stable at room temperature. The radiative lifetimes of XX are estimated to be of the same order than those of X.

The codes associated with our VQMC model have been provided along with this work, and can be readily used to investigate XX in NPLs built of different materials, by simply changing the input effective masses, dielectric constants and NPL dimensions.

Author Contributions

JP developed the VQMC model (methodology). DMP and JP implemented the computational code (software). DMP ran the simulations (data curation) and analyzed the results under supervision of JIC. The results were discussed by all the authors. JIC and DMP wrote the original draft of manuscript. JIC was in charge of reviewing and editing the final manuscript.

Conflicts of interest

The authors declare no competing financial interests.

Acknowledgements

Finacial support from MINECO project CTQ2017-83781-P (JP,JIC), the European Research Council (ERC) via Consolidator Grant 724424-No-LIMIT (D.M-P.), Generalitat Valenciana via Prometeo Grant Q-Devices (Prometeo/2018/098) and Universitat Jaume I (UJI) B-2021-06 project is gratefully acknowledged.

Notes and references

1 K. Chen, C. Wang, Z. Peng, K. Qi, Z. Guo, Y. Zhang and H. Zhang, *Coordination Chemistry Reviews*, 2020, **418**, 213333.

2 D. Porotnikov and M. Zamkov, *The Journal of Physical Chemistry C*, 2020, **124**, 21895–21908.

3 M. Nasilowski, B. Mahler, E. Lhuillier, S. Ithurria and B. Dubertret, *Chemical reviews*, 2016, **116**, 10934–10982.

4 M. Sharma, S. Delikanli and H. V. Demir, *Proceedings of the IEEE*, 2019, **108**, 655–675.

5 B. T. Diroll, *Journal of Materials Chemistry C*, 2020, **8**, 10628–10640.

6 L. T. Kunneman, M. D. Tessier, H. Heuclin, B. Dubertret, Y. V. Aulin, F. C. Grozema, J. M. Schins and L. D. Siebbeles, *The Journal of Physical Chemistry Letters*, 2013, **4**, 3574–3578.

7 Q. Li and T. Lian, *Nano letters*, 2017, **17**, 3152–3158.

8 J. P. Philbin, A. Brumberg, B. T. Diroll, W. Cho, D. V. Talapin, R. D. Schaller and E. Rabani, *The Journal of Chemical Physics*, 2020, **153**, 054104.

9 E. Benjamin, V. J. Yallapragada, D. Amgar, G. Yang, R. Tenne and D. Oron, *The journal of physical chemistry letters*, 2020, **11**, 6513–6518.

10 J. Q. Grim, S. Christodoulou, F. Di Stasio, R. Krahne, R. Cingolani, L. Manna and I. Moreels, *Nature nanotechnology*, 2014, **9**, 891–895.

11 J. Chen, Q. Zhang, J. Shi, S. Zhang, W. Du, Y. Mi, Q. Shang, P. Liu, X. Sui, X. Wu *et al.*, *Communications Physics*, 2019, **2**, 1–8.

12 B. R. C. Vale, E. Socie, A. Burgos-Caminal, J. Bettini, M. A. Schiavon and J.-E. Moser, *The Journal of Physical Chemistry Letters*, 2020, **11**, 387–394.

13 L. Peng, W. Cho, X. Zhang, D. Talapin and X. Ma, *Physical Review Materials*, 2021, **5**, L051601.

14 X. Ma, B. T. Diroll, W. Cho, I. Fedin, R. D. Schaller, D. V. Talapin, S. K. Gray, G. P. Wiederrecht and D. J. Gosztola, *ACS nano*, 2017, **11**, 9119–9127.

15 F. G. Flórez, L. D. Siebbeles and H. Stoof, *Physical Review B*, 2020, **102**, 115302.

16 Y. Gao, M. Li, S. Delikanli, H. Zheng, B. Liu, C. Dang, T. C. Sum and H. V. Demir, *Nanoscale*, 2018, **10**, 9466–9475.

17 S. Tomić, J. M. Miloszewski, E. J. Tyrrell and D. J. Binks, 2015 IEEE 42nd Photovoltaic Specialist Conference (PVSC), 2015, pp. 1–4.

18 R. M. Stevenson, R. J. Young, P. Atkinson, K. Cooper, D. A. Ritchie and A. J. Shields, *Nature*, 2006, **439**, 179–182.

19 O. Akimoto and E. Hanamura, *Journal of the Physical Society of Japan*, 1972, **33**, 1537–1544.

20 W. Brinkman, T. Rice and B. Bell, *Physical Review B*, 1973, **8**, 1570.

21 D. Kleinman, *Physical Review B*, 1983, **28**, 871.

22 D. Birkedal, J. Singh, V. Lyssenko, J. Erland and J. M. Hvam, *Physical review letters*, 1996, **76**, 672.

23 J. Haynes, *Physical Review Letters*, 1960, **4**, 361.

24 J. Singh, D. Birkedal, V. Lyssenko and J. M. Hvam, *Physical Review B*, 1996, **53**, 15909.

25 I.-K. Oh and J. Singh, *Physical Review B*, 1999, **60**, 2528.

26 G. Moody, R. Singh, H. Li, I. Akimov, M. Bayer, D. Reuter,

A. Wieck, A. Bracker, D. Gammon and S. Cundiff, *Physical Review B*, 2013, **87**, 041304.

27 S. J. Vonk, B. A. Heemskerk, R. C. Keitel, S. O. Hinterding, J. J. Geuchies, A. J. Houtepen and F. T. Rabouw, *Nano Letters*, 2021, **21**, 5760–5766.

28 Y. You, X.-X. Zhang, T. C. Berkelbach, M. S. Hybertsen, D. R. Reichman and T. F. Heinz, *Nature Physics*, 2015, **11**, 477–481.

29 K. A. Velizhanin and A. Saxena, *Physical Review B*, 2015, **92**, 195305.

30 J. Yu and R. Chen, *InfoMat*, 2020, **2**, 905–927.

31 J. Shumway, A. Franceschetti and A. Zunger, *Physical Review B*, 2001, **63**, 155316.

32 F. Rajadell, J. I. Climente and J. Planelles, *Physical Review B*, 2017, **96**, 035307.

33 M. Richter, *Physical Review Materials*, 2017, **1**, 016001.

34 J. Planelles and J. I. Climente, *Computer Physics Communications*, 2021, **261**, 107782.

35 D. F. Macias-Pinilla, J. Planelles, I. Mora-Seró and J. I. Climente, *The Journal of Physical Chemistry C*, 2021, **125**, 15614–15622.

36 T. F. Rønnow, T. G. Pedersen and B. Partoens, *Physical Review B*, 2012, **85**, 045412.

37 S. Christodoulou, J. I. Climente, J. Planelles, R. Brescia, M. Prato, B. Martín-García, A. H. Khan and I. Moreels, *Nano letters*, 2018, **18**, 6248–6254.

38 M. Kumagai and T. Takagahara, *Physical Review B*, 1989, **40**, 12359.

39 L. Jacak, P. Hawrylak and A. Wojs, *Quantum Dots*, Springer, 1998.

40 D. F. Macias-Pinilla, C. Echeverría-Arrondo, A. F. Gualdrón Reyes, S. Agouram, V. Muñoz-Sanjosé, J. Planelles, I. Mora-Seró and J. I. Climente, *Chemistry of Materials*, 2021, **33**, 420–429.

41 S. Adachi, *Handbook on physical properties of semiconductors*, Springer Science & Business Media, 2004, vol. 2.

42 R. Benchamekh, N. A. Gippius, J. Even, M. Nestoklon, J.-M. Jancu, S. Ithurria, B. Dubertret, A. L. Efros and P. Voisin, *Physical Review B*, 2014, **89**, 035307.

43 A. Chernikov, T. C. Berkelbach, H. M. Hill, A. Rigosi, Y. Li, O. B. Aslan, D. R. Reichman, M. S. Hybertsen and T. F. Heinz, *Physical review letters*, 2014, **113**, 076802.

44 A. W. Achtstein, A. Schliwa, A. Prudnikau, M. Hardzei, M. V. Artemyev, C. Thomsen and U. Woggon, *Nano letters*, 2012, **12**, 3151–3157.

45 R. Benchamekh, N. A. Gippius, J. Even, M. O. Nestoklon, J.-M. Jancu, S. Ithurria, B. Dubertret, A. L. Efros and P. Voisin, *Phys. Rev. B*, 2014, **89**, 035307.

46 S. Ayari, M. T. Quick, N. Owschimikow, S. Christodoulou, G. H. Bertrand, M. Artemyev, I. Moreels, U. Woggon, S. Jaziri and A. W. Achtstein, *Nanoscale*, 2020, **12**, 14448–14458.

47 E. V. Shornikova, D. R. Yakovlev, N. A. Gippius, G. Qiang, B. Dubertret, A. H. Khan, A. Di Giacomo, I. Moreels and M. Bayer, *Nano Letters*, 2021, **21**, 10525–10531.

48 E. A. Hylleraas and A. Ore, *Physical Review*, 1947, **71**, 493.

49 A. Piryatinski, S. A. Ivanov, S. Tretiak and V. I. Klimov, *Nano letters*, 2007, **7**, 108–115.

50 S. Ithurria, M. Tessier, B. Mahler, R. Lobo, B. Dubertret and A. L. Efros, *Nature materials*, 2011, **10**, 936–941.

51 A. Di Giacomo, C. Rodà, A. H. Khan and I. Moreels, *Chemistry of Materials*, 2020, **32**, 9260–9267.

52 G. H. Bertrand, A. Polovitsyn, S. Christodoulou, A. H. Khan and I. Moreels, *Chemical Communications*, 2016, **52**, 11975–11978.

53 A. W. Achtstein, A. Antanovich, A. Prudnikau, R. Scott, U. Woggon and M. Artemyev, *The Journal of Physical Chemistry C*, 2015, **119**, 20156–20161.

54 S. J. Zelewski, K. C. Nawrot, A. Zak, M. Gladysiewicz, M. Nyk and R. Kudrawiec, *The journal of physical chemistry letters*, 2019, **10**, 3459–3464.

55 A. Naeem, F. Masia, S. Christodoulou, I. Moreels, P. Borri and W. Langbein, *Physical Review B*, 2015, **91**, 121302.

56 J. Planelles, A. W. Achtstein, R. Scott, N. Owschimikow, U. Woggon and J. I. Climente, *ACS Photonics*, 2018, **5**, 3680–3688.

57 J. Feldmann, G. Peter, E. Göbel, P. Dawson, K. Moore, C. Foxon and R. Elliott, *Physical review letters*, 1987, **59**, 2337.

58 P. Geiregat, C. Rodá, I. Tanghe, S. Singh, A. Di Giacomo, D. Lebrun, G. Grimaldi, J. Maes, D. Van Thourhout, I. Moreels *et al.*, *Light: Science & Applications*, 2021, **10**, 1–11.